LETTER

Maternal imprinting at the *H19–Igf2* locus maintains adult haematopoietic stem cell quiescence

Aparna Venkatraman[1,2], Xi C. He[1], Joanne L. Thorvaldsen[3], Ryohichi Sugimura[1], John M. Perry[1], Fang Tao[1], Meng Zhao[1], Matthew K. Christenson[1], Rebeca Sanchez[1,4], Jaclyn Y. Yu[1], Lai Peng[5], Jeffrey S. Haug[1], Ariel Paulson[1], Hua Li[1], Xiao–bo Zhong[5], Thomas L. Clemens[6], Marisa S. Bartolomei[3] & Linheng Li[1,7]

The epigenetic regulation of imprinted genes by monoallelic DNA methylation of either maternal or paternal alleles is critical for embryonic growth and development[1]. Imprinted genes were recently shown to be expressed in mammalian adult stem cells to support self-renewal of neural and lung stem cells[2–4]; however, a role for imprinting per se in adult stem cells remains elusive. Here we show upregulation of growth-restricting imprinted genes, including in the *H19–Igf2* locus[5], in long-term haematopoietic stem cells and their downregulation upon haematopoietic stem cell activation and proliferation. A differentially methylated region upstream of *H19* (H19-DMR), serving as the imprinting control region, determines the reciprocal expression of *H19* from the maternal allele and *Igf2* from the paternal allele[1]. In addition, *H19* serves as a source of miR-675, which restricts *Igf1r* expression[6]. We demonstrate that conditional deletion of the maternal but not the paternal H19-DMR reduces adult haematopoietic stem cell quiescence, a state required for long-term maintenance of haematopoietic stem cells, and compromises haematopoietic stem cell function. Maternal-specific H19-DMR deletion results in activation of the Igf2–Igfr1 pathway, as shown by the translocation of phosphorylated FoxO3 (an inactive form) from nucleus to cytoplasm and the release of FoxO3-mediated cell cycle arrest, thus leading to increased activation, proliferation and eventual exhaustion of haematopoietic stem cells. Mechanistically, maternal-specific H19-DMR deletion leads to *Igf2* upregulation and increased translation of Igf1r, which is normally suppressed by *H19*-derived miR-675. Similarly, genetic inactivation of *Igf1r* partly rescues the H19-DMR deletion phenotype. Our work establishes a new role for this unique form of epigenetic control at the *H19–Igf2* locus in maintaining adult stem cells.

Our earlier studies showed that imprinted genes, including those within the *H19–Igf2* locus (Fig. 1a), are differentially expressed in haematopoietic stem and progenitor cells (HSPCs)[7]. To explore this further, we systematically analysed imprinted gene expression in quiescent-enriched long-term haematopoietic stem cells (LT-HSCs), more active short-term (ST)-HSCs and multipotent progenitor (MPP) populations (Fig. 1b)[8]. Out of 88 imprinted genes, 23 were differentially expressed in these populations. Of these 23, 15 were preferentially expressed in LT-HSCs, whereas the others were predominantly expressed in ST-HSCs and MPPs (Fig. 1c). Intriguingly, 80% of the imprinted genes with predominant expression in LT-HSCs were associated with growth restriction, including *H19*, *Cdkn1c/p57*, *Ndn*, *Rb*, *Gtl2* and *Grb10* (ref. 9). In contrast, imprinted genes expressed preferentially in ST-HSCs and MPPs, including *Ascl2*, *Peg12*, *Sfmbt2*, *Pon3*, *Atp10a* and *Osbpl5*, were associated with growth promotion and increased metabolism[10] (see quantitative real-time PCR assay in Supplementary Fig. 1a).

Given the critical role of *H19* during embryonic development and its preferential expression in LT-HSCs, we considered that it plays a role

in restricting LT-HSC activation. To test this idea, we conditionally deleted H19-DMR (an epigenetic regulator that controls expression of *H19*) by breeding *H19*^flDMR/flDMR^ mice with *Mx1-Cre* mice to generate maternal (m*H19*^ΔDMR/+^) and paternal (p*H19*^ΔDMR/+^) allele-specific mutants (Supplementary Fig. 1b). The *DMR* region was deleted with 100% efficiency in LT-HSC (Supplementary Fig. 1c, e–g)[11]. As early as 6 weeks, flow cytometric analysis showed a substantial decrease in frequency and absolute number of LT-HSCs in m*H19*^ΔDMR/+^ mice (Fig. 1 d–f and Supplementary Fig. 1d), but not in p*H19*^ΔDMR/+^ mice (Fig. 1e and Supplementary Fig. 2a, b). Concurrently, we observed a significant increase in frequency and absolute number of ST-HSCs (Fig. 1d–f); however, the total number of bone marrow cells remained unchanged (Fig. 1g). By 6 months, both LT- and ST-HSCs were significantly decreased in frequency and absolute number, whereas bone marrow cellularity increased only in m*H19*^ΔDMR/+^ mice (Fig. 1d–g and Supplementary Fig. 2c, d).

Cell cycle analysis of LT-HSCs at 6 weeks after pIpC induction showed a decrease in the G0 phase fraction and a concomitant increase in the G1 phase fraction in m*H19*^ΔDMR/+^ relative to control (Fig. 1h–j). We then tested the response of m*H19*^ΔDMR/+^ mice to bone marrow damage by administering 5-fluorouracil (5FU), which eliminates active HSPCs while sparing quiescent HSCs. Surviving quiescent HSCs later replenish lost HSPCs[12] (Fig. 1k). In this context, a significant reduction in quiescent HSCs after three cycles of 5FU treatment led to deficient bone marrow recovery in the m*H19*^ΔDMR/+^ mutant compared with control (Fig. 1l, m and Supplementary Fig. 2f). Altogether, maternal but not paternal deletion of H19-DMR resulted in loss of HSC quiescence, leading to progressive loss of LT-HSCs and then ST-HSCs, accompanied by increasing progenitor cell proliferation and differentiation, thus ultimately increasing total bone marrow cellularity (Fig. 1g and Supplementary Figs 2e and 3a–d).

To characterize the phenotype functionally, we transplanted equal numbers of sorted LT-HSCs from mutants and their control littermates. We observed a significant reduction in reconstitution ability for LT-HSCs derived from m*H19*^ΔDMR/+^ but not p*H19*^ΔDMR/+^ mutants compared with controls. Although overall engraftment was reduced in primary and secondary recipients, no mature lineage bias was apparent (Fig. 2a–f). Limiting dilution analysis to quantify functional HSCs showed a 2.5-fold decrease in m*H19*^ΔDMR/+^ mutant HSCs relative to control (Fig. 2d). Reciprocal transplantation of wild-type donor cells into either m*H19*^ΔDMR/+^ or control recipients did not result in alterations in haematopoiesis (Fig. 2g, h), indicating that an intrinsic change in the m*H19*^ΔDMR/+^ mutant HSCs was the primary cause of the phenotype.

Next, we investigated whether H19-DMR controls the imprinted expression of *H19* and *Igf2* from the maternal and paternal alleles, respectively, in adult HSCs, as is observed in embryos[11]. Our RNA-seq analysis showed differential expression of *H19* as well as *Igf2* in

[1]Stowers Institute for Medical Research, Kansas City, Missouri 64110, USA. [2]Centre for Stem Cell Research, Christian Medical College, Vellore 632002, India. [3]Department of Cell & Developmental Biology, University of Pennsylvania, Philadelphia, Pennsylvania 19104, USA. [4]Cell Therapy and Genetics Laboratory, Institute de Recerca Vall d'hebron, Barcelona 08035, Spain. [5]Department of Pharmacology, Toxicology & Therapeutics, University of Kansas Medical Center, Kansas City, Kansas 66160, USA. [6]Center for Musculoskeletal Research, Johns Hopkins Medicine, Baltimore, Maryland 21287, USA. [7]Department of Pathology & Laboratory Medicine, University of Kansas Medical Center, Kansas City, Kansas 66160, USA.
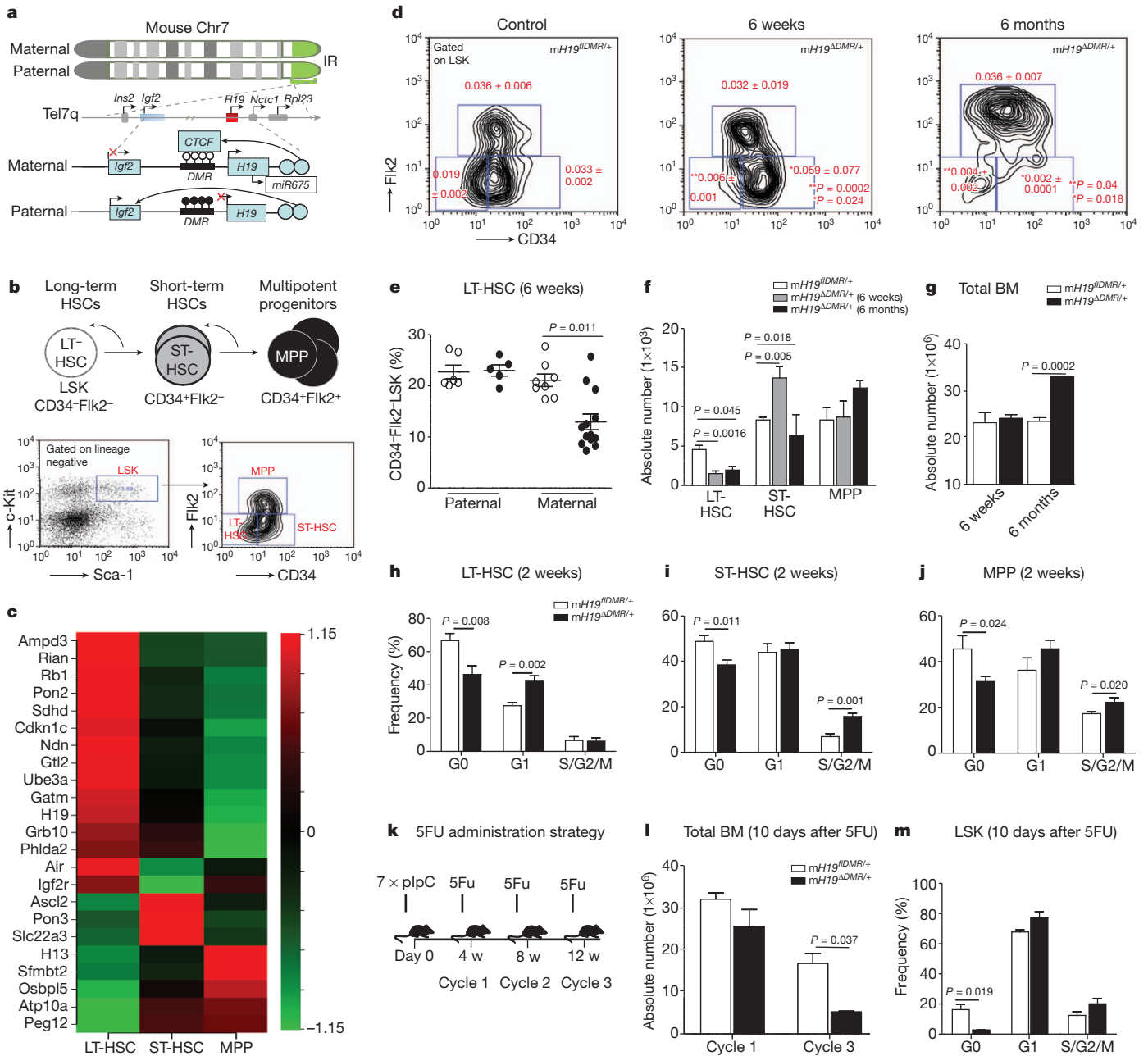
Figure 1 | Defective LT-HSCs in m$H19^{\Delta DMR/+}$ mice. a, H19–Igf2 cluster. Top: red box, maternally expressed; blue box, paternally expressed; grey boxes, genes in the cluster. Bottom: unmethylated (open circles) and methylated (filled circles) CpG dinucleotides; red cross, no expression; arrow, active transcription. IR, imprinting region. **b**, Upper cartoon, hierarchical organization. Curved arrow, self-renewal. Lower image: fluorescence-activated cell sorting (FACS) plot. Left panel: gated on LSK; right panel: on CD34 and FLk2. **c**, Heat map of imprinted genes ($n = 3$). **d**, FACS plot of m$H19^{\Delta DMR/+}$ ($n = 9$) and m$H19^{flDMR/+}$ ($n = 8$). Asterisks and double asterisks, significant compared with control. **e**, Percentage of LT-HSCs of LSK. Absolute numbers of (**f**) HSCs and (**g**) total bone marrow cells. **h–j**, Cell cycle analysis 2 weeks after pIpC induction ($n = 5$). **k**, 5FU cycles. **l**, Total bone marrow cells ($n = 3$). **m**, Cell cycle analysis. Error bars, s.e.m.

HSCs (Fig. 3a, b). By crossing $H19^{flDMR/+}$ females with *Mus castaneus* (Cast) males, which enables parental allele-discrimination by single nucleotide polymorphism analysis, we further detected exclusive expression of *Igf2* from the paternal allele in HSCs (Fig. 3c). However, after deletion of the maternal H19-DMR, we detected *H19* downregulation and *Igf2* upregulation, which resulted from biallelic *Igf2* expression in HSCs (Fig. 3d–f). *Igf2* was similarly upregulated in bone marrow, including surrounding stromal cells, after maternal deletion of H19-DMR (Fig. 3g, h). However, as shown by reciprocal transplantation, an extrinsic increase of *Igf2* expression alone is not sufficient to cause the m$H19^{\Delta DMR/+}$ HSC phenotype. We next investigated whether the *Igf2* signalling[13] pathway is activated in m$H19^{\Delta DMR/+}$ LT-HSCs. Binding of

Igf2 to Igf1r activates signalling, whereas Igf2 binding to Igf2r attenuates signalling[14]. Igf2 and Igf1r amounts were gradually increased from LT-HSCs to MPPs (Fig. 3i, j). However, messenger RNA (mRNA), protein concentrations, and the number of Igf1r$^+$ cells were significantly increased in m$H19^{\Delta DMR/+}$ LT-HSCs compared with controls (Fig. 3k–m), with no change in *Igf2*r expression (Fig. 3k). Igf2–Igf1r signalling is known to activate PI3K-Akt, which phosphorylates and inactivates FoxO3, a transcription factor that arrests the cell cycle[15,16]. Inactive pFoxO3 was detected in only 15% of normal LT-HSCs but was substantially increased in ST-HSCs and MPPs (Fig. 3n, o); however, in m$H19^{\Delta DMR/+}$ pFoxO3 was detected in 75% of LT-HSCs. Our data indicate that H19-DMR deletion increased Igf2
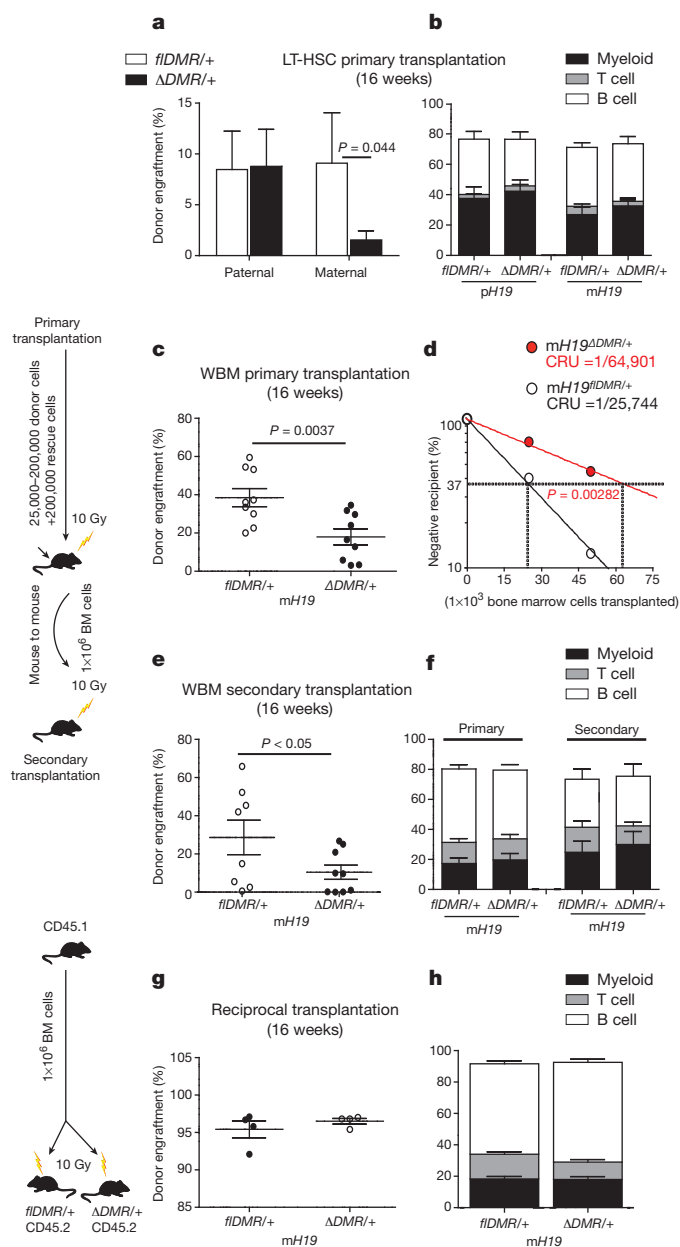
Figure 2 | Compromised HSC function in m*H19*$^{\Delta DMR/+}$ mice. Competitive re-population assay 16 weeks after transplantation in (**a**) sorted 100 LT-HSCs (*n* = 10), (**c**) primary transplant (test dosage of 2 × 10⁵ bone marrow cells) (*n* = 10), (**e**) secondary transplant (*n* = 10), (**g**) reciprocal transplantation (*n* = 4). **d**, Competitive re-population unit (CRU) content in each group of mice transplanted at each dose (*n* = 60 mice in total). Horizontal dotted line, 37% of recipient mice failed to engraft; vertical dotted lines, various CRU frequencies for each condition. Donor-derived lineage analysis after (**b**) primary transplantation, (**f**) secondary transplantation, (**h**) reciprocal transplantation. Error bars, s.e.m.

signalling, which released FoxO3-mediated suppression of HSC activation and proliferation.

In the placenta, *H19* functions as a precursor of miR-675, which in turn suppresses Igf1r[6]. We next investigated whether this regulation exists in adult HSCs. Expression of miR-675 was highest in LT-HSCs in the control mice but was substantially reduced in m*H19*$^{\Delta DMR/+}$ LT-HSCs (Fig. 4a). To explore the potential role of miR-675 in Igf1r regulation, we transplanted bone marrow cells overexpressing miR-675 into wild-type mice. Overexpression of miR-675 increased the percentage of quiescent CD34⁻ lineage⁻Sca-1⁺cKit⁺ (LSK) cells but did not significantly affect active CD34⁺ LSK cells (Fig. 4b). Western
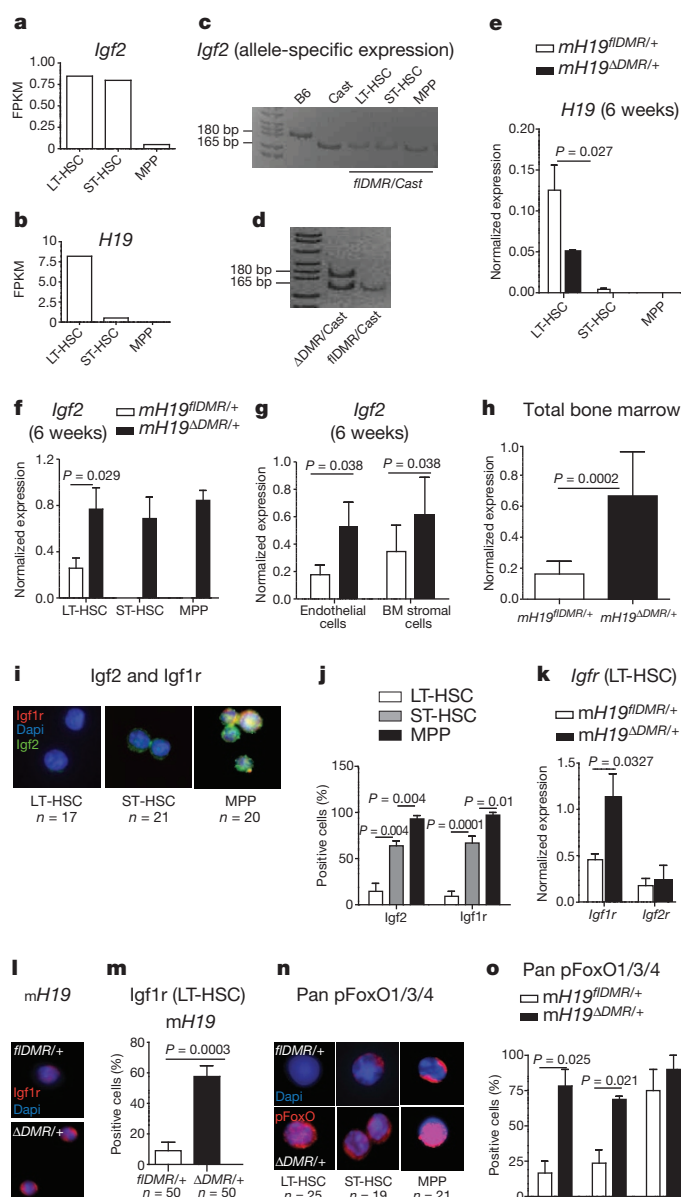
Figure 3 | Activation of Igf2–FoxO3 signalling in m*H19*$^{\Delta DMR/+}$ mice.
a, b, RNA-seq analysis of *Igf2* and *H19* transcripts. FPKM, fragments per kilobase of exon per million fragments mapped. **c, d**, Allele-specific expression of the *Igf2* transcript. Quantitative (q)RT-PCR 6 weeks after pIpC induction (*n* = 3) for (**e**) *H19*, (**f**) *Igf2*, (**g**) stromal cells and (**h**) total bone marrow (*n* = 5). **i, j**, Single-cell Igf1r and Igf2 staining from wild-type bone marrow cells and its quantification (*n* = 4). **k**, *Igf1r* and *Igf2r* expression in sorted LT-HSCs. **l, m**, Igf1r immunostaining and its quantification (*n* = 4). **n, o**, Single-cell phospho-FoxO1/3/4 staining and its quantification (*n* = 4). Scale bar, 10 μm. Error bars, s.e.m.

blot analysis showed a significant reduction of Igf1r by miR-675 compared with control (Fig. 4c). Furthermore, Igf1r amounts were lower in CD34⁻ LSK compared with CD34⁺ LSK cells in the control. However, miR-675 overexpression significantly decreased Igf1r (Fig. 4c–e). These data demonstrate that *H19*-derived miR-675 regulates Igf1r and the corresponding quiescent state in HSCs.

To confirm further that H19-DMR controls Igf2–Igf1r signalling, we crossed female *H19*$^{flDMR/+}$ mice with male *Mx1-Cre:Igf1r*$^{fl/fl}$ mice (Supplementary Fig. 4a)[17]. Although m*H19*$^{\Delta DMR/+}$ mutants (Fig. 3f, g) showed a decrease in LT-HSCs and an increase in ST-HSCs and MPPs, *Igf1r*$^{-/-}$ mutants showed an increase in LT-HSCs and a decrease in MPPs. This indicates that Igf1r regulates the transitions from LT-HSCs to ST-HSCs and further to MPPs. Interestingly, m*H19*$^{\Delta DMR/+}$*Igf1r*$^{-/-}$
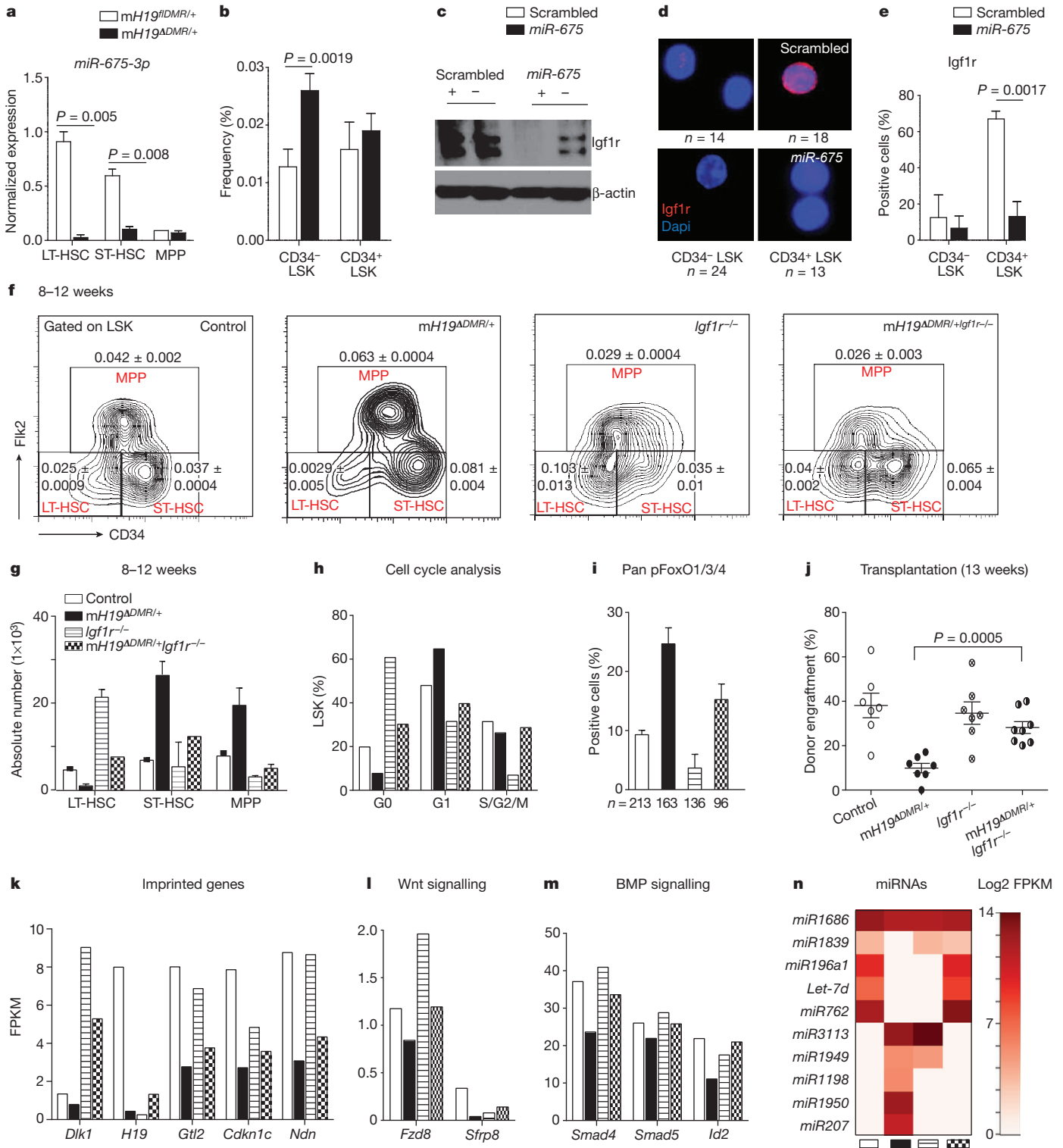
Figure 4 | Igf1r regulation and rescue by genetic blockage of Igf2–Igf1r signalling. a, miR-675 analysis by qRT–PCR ($n = 3$). **b**, Frequency of CD34⁻ versus CD34⁺ LSK cells 8 weeks after lentiviral infection. **c**, Immunoblot analysis of Igf1r in sorted bone marrow cells (positive and negative for green fluorescent protein (GFP)). **d, e**, Single-cell immunostaining of Igf1r 8 weeks after lentiviral infection and its quantification ($n = 4$). **f**, Representative FACS plot with frequency ($n = 4$), (**g**) absolute number and (**h**) cell cycle analysis. **i**, Pan-pFoxO staining ($n = 3$). **j**, Donor engraftment 13 weeks after transplantation. RNA sequencing analysis in sorted stem cells: **k**, imprinted genes; **l, m**, Wnt and BMP signalling; **n**, heat map of miRNA expression. Error bars, s.e.m.

double mutants showed a partial restoration of LT-HSC frequency (Fig. 4f), whereas the transition from ST-HSCs to MPPs was still blocked (Fig. 4f, g). This indicates that Igf2–Igf1r signalling is partly responsible for the m$H19^{\Delta DMR/+}$ phenotype. An increase in ST-HSC frequency in double-mutant mice was probably due to blocked transition from ST-HSC to MPP by downregulation of Igf1r. Furthermore, cell cycle analysis

and pFoxO3 staining in double mutants showed partial rescue of the loss of quiescence phenotype (Fig. 4h, i).

To demonstrate phenotypic rescue functionally in m$H19^{\Delta DMR/+}$ $Igf1r^{-/-}$ mice, we performed bone marrow transplantation assays. Although m$H19^{\Delta DMR/+}$ mutants had significantly reduced engraftment due to LT-HSC loss, engraftment of m$H19^{\Delta DMR/+} Igf1r^{-/-}$ bone

marrow cells increased to an amount between that of the m$H19^{ADMR/+}$ and the $Igf1r^{-/-}$ single mutants, indicating a partial functional rescue (Fig. 4j and Supplementary Fig. 4b). These results indicate that the maternal H19-DMR controls Igf2–Igf1r signalling which regulates HSC state; however, the partial rescue indicates that deletion of H19-DMR also affects other pathways required for LT-HSC maintenance. To investigate this possibility, we performed RNA-seq analysis of HSCs isolated from control, m$H19^{ADMR}$ single, $Igf1r^{-/-}$ single and m$H19^{ADMR/+}$:$Igf1r^{-/-}$ double mutants. m$H19^{ADMR/+}$ HSPCs showed widespread alterations in expression of imprinted genes in all three populations (Supplementary Figs 4c and 5). Genes involved in cell cycle arrest (*Cdkn1c*)[18,19], tumour suppression and stem cell maintenance (*Ndn, Gtl2*)[20,21] were downregulated in LT-HSCs. However, $Igf1r^{-/-}$ LT-HSCs largely maintained expression patterns similar to control, with high expression amounts of *Cdkn1c, Ndn, Gtl2* and *Dlk1*. The double mutants generally showed partial rescue of the alterations observed in single mutants, indicating either compensation in gene expression and/or existence of a proposed imprinted gene network[22,23] (Fig. 4k and Supplementary Fig. 4c). Gene expression profiling of non-imprinted genes showed many overlapping downstream genes and microRNA (miRNAs) that were abnormally expressed in single mutants but partly rescued in double mutants (Fig. 4l–n and Supplementary Figs 6a–c and 7e). These included components of the Wnt and Tgf-β/BMP pathways such as *Smad4, Id2* and *Fzd8* (refs 24–27) as well as *Let-7*, which is known to repress cell proliferation[28] and Igf signalling[29] (Fig. 4l–n). Interestingly, H19-DMR potentially controls other miRNAs, small nucleolar RNAs (SnoRNAs) and genes (*Dusp26, p2rx2* and *Gpr63*) independent of the Igf2–Igf1r signalling (Supplementary Fig. 7a–f), with a known function for *Dusp26* in inhibiting cell proliferation[30]. Taken together, our data show that maternal H19-DMR primarily restricts Igf2–Igf1r signalling, but also influences other genes and miRNAs involved in maintaining HSC quiescence.

By studying the H19-DMR locus in an allele-specific manner, we demonstrate that a specialized form of epigenetic control—genomic imprinting—is critical to the maintenance of adult stem cells. This is accomplished by maintaining LT-HSC quiescence, which can be attributed largely to Igf2–Igf1r-dependent signalling, but also to extra Igf2–Igf1r-independent effects on the regulation of cell cycle, proliferation and growth.

METHODS SUMMARY

Genotyping primers, flow assays and immunostaining were reported previously[15,26]. Lentivirus-mediated transfection used Magnetofection^{TM} and ViroMag R/L particles (OZ Biosciences). Microarray and RNA-seq analyses used Affymetrix MouseGenome430_2 arrays and Illumina TruSeq RNA Sample Prep Kit (catalogue number FC-122-1001) respectively, followed by sequencing on an Illumina HiSeq 2000. Statistical analyses were performed (pairwise comparisons were performed using a Student's *t*-test) in Prism 5 GraphPad.

Full Methods and any associated references are available in the online version of the paper.

1. Bartolomei, M. S. Genomic imprinting: employing and avoiding epigenetic processes. *Genes Dev.* **23,** 2124–2133 (2009).
2. Berg, J. S. *et al.* Imprinted genes that regulate early mammalian growth are coexpressed in somatic stem cells. *PLoS ONE* **6,** e26410 (2011).
3. Ferrón, S. R. *et al.* Postnatal loss of *Dlk1* imprinting in stem cells and niche astrocytes regulates neurogenesis. *Nature* **475,** 381–385 (2011).
4. Zacharek, S. J. *et al.* Lung stem cell self-renewal relies on BMI1-dependent control of expression at imprinted loci. *Cell Stem Cell* **9,** 272–281 (2011).
5. DeChiara, T. M., Robertson, E. J. & Efstratiadis, A. Parental imprinting of the mouse insulin-like growth factor II gene. *Cell* **64,** 849–859 (1991).
6. Keniry, A. *et al.* The H19 lincRNA is a developmental reservoir of miR-675 that suppresses growth and Igf1r. *Nature Cell Biol.* **14,** 659–665 (2012).
7. Haug, J. S. *et al.* N-cadherin expression level distinguishes reserved versus primed states of hematopoietic stem cells. *Cell Stem Cell* **2,** 367–379 (2008).
8. Yang, L. *et al.* Identification of Lin⁻Sca1⁺kit⁺CD34⁻Flt3- short-term hematopoietic stem cells capable of rapidly reconstituting and rescuing myeloablated transplant recipients. *Blood* **105,** 2717–2723 (2005).
9. Frost, J. M. & Moore, G. E. The importance of imprinting in the human placenta. *PLoS Genet.* **6,** e1001015 (2010).
10. Hudson, Q. J., Kulinski, T. M., Huetter, S. P. & Barlow, D. P. Genomic imprinting mechanisms in embryonic and extraembryonic mouse tissues. *Heredity* **105,** 45–56 (2010).
11. Thorvaldsen, J. L., Fedoriw, A. M., Nguyen, S. & Bartolomei, M. S. Developmental profile of H19 differentially methylated domain (DMD) deletion alleles reveals multiple roles of the DMD in regulating allelic expression and DNA methylation at the imprinted H19/Igf2 locus. *Mol. Cell. Biol.* **26,** 1245–1258 (2006).
12. Lerner, C. & Harrison, D. E. 5-Fluorouracil spares hemopoietic stem cells responsible for long-term repopulation. *Exp. Hematol.* **18,** 114–118 (1990).
13. Smith, F. M., Garfield, A. S. & Ward, A. Regulation of growth and metabolism by imprinted genes. *Cytogenet. Genome Res.* **113,** 279–291 (2006).
14. Kang, H. M., Park, S. & Kim, H. Insulin-like growth factor 2 enhances insulinogenic differentiation of human eyelid adipose stem cells via the insulin receptor. *Cell Prolif.* **44,** 254–263 (2011).
15. Zhang, J. *et al.* PTEN maintains haematopoietic stem cells and acts in lineage choice and leukaemia prevention. *Nature* **441,** 518–522 (2006).
16. Tothova, Z. *et al.* FoxOs are critical mediators of hematopoietic stem cell resistance to physiologic oxidative stress. *Cell* **128,** 325–339 (2007).
17. Klinakis, A. *et al.* Igf1r as a therapeutic target in a mouse model of basal-like breast cancer. *Proc. Natl Acad. Sci. USA* **106,** 2359–2364 (2009).
18. Zou, P. *et al.* p57(Kip2) and p27(Kip1) cooperate to maintain hematopoietic stem cell quiescence through interactions with Hsc70. *Cell Stem Cell* **9,** 247–261 (2011).
19. Walkley, C. R., Shea, J. M., Sims, N. A., Purton, L. E. & Orkin, S. H. Rb regulates interactions between hematopoietic stem cells and their bone marrow microenvironment. *Cell* **129,** 1081–1095 (2007).
20. Kubota, Y., Osawa, M., Jakt, L. M., Yoshikawa, K. & Nishikawa, S. Necdin restricts proliferation of hematopoietic stem cells during hematopoietic regeneration. *Blood* **114,** 4383–4392 (2009).
21. Stadtfeld, M. *et al.* Aberrant silencing of imprinted genes on chromosome 12qF1 in mouse induced pluripotent stem cells. *Nature* **465,** 175–181 (2010).
22. Zhao, Z. *et al.* Circular chromosome conformation capture (4C) uncovers extensive networks of epigenetically regulated intra- and interchromosomal interactions. *Nature Genet.* **38,** 1341–1347 (2006).
23. Varrault, A. *et al.* Zac1 regulates an imprinted gene network critically involved in the control of embryonic growth. *Dev. Cell* **11,** 711–722 (2006).
24. Karlsson, G. *et al.* Smad4 is critical for self-renewal of hematopoietic stem cells. *J. Exp. Med.* **204,** 467–474 (2007).
25. Sugimura, R. *et al.* Noncanonical wnt signaling maintains hematopoietic stem cells in the niche. *Cell* **150,** 351–365 (2012).
26. Perry, J. M. *et al.* Cooperation between both Wnt/β-catenin and PTEN/PI3K/Akt signaling promotes primitive hematopoietic stem cell self-renewal and expansion. *Genes Dev.* **25,** 1928–1942 (2011).
27. Dijke, P. & Heldin, C. H. *Smad Signal Transduction: Smads in Proliferation, Differentiation and Disease* (Springer, 2006).
28. Johnson, C. D. *et al.* The let-7 microRNA represses cell proliferation pathways in human cells. *Cancer Res.* **67,** 7713–7722 (2007).
29. Toledano, H., D'Alterio, C., Czech, B., Levine, E. & Jones, D. L. The let-7-Imp axis regulates ageing of the *Drosophila* testis stem-cell niche. *Nature* **485,** 605–610 (2012).
30. Yu, W. *et al.* A novel amplification target, DUSP26, promotes anaplastic thyroid cancer cell growth by inhibiting p38 MAPK activity. *Oncogene* **26,** 1178–1187 (2007).

Author Contributions A.V. performed experiments, analysed data and wrote the manuscript. X.H. provided training, performed transplantations and RNA-seq. F.T., J.T., M.C., L.P., X.Z., A.P., H.L., J.P. M.Z., J.H. and T.C. performed part of the experiments. M.B. contributed the mouse lines. L.L. directed the overall project and co-wrote the manuscript. All authors contributed to reading and editing the manuscript.

Author Information The microarray and RNA-seq data have been deposited in ArrayExpress under accession numbers E-MTAB-1644 and E-MTAB-1628, respectively. Reprints and permissions information is available at www.nature.com/reprints. The authors declare no competing financial interests. Readers are welcome to comment on the online version of the paper. Correspondence and requests for materials should be addressed to L. Li (lil@stowers.org).

METHODS

Animals. All mice used in this study were housed in the animal facility at the Stowers Institute for Medical Research and handled according to the guidelines of the Institute and the National Institutes of Health. All procedures were approved by the Institutional Animal Care and Use Committee of the Stowers Institute. *H19-DMR*$^{flDMR/flDMR}$ mice on B6 background were provided by M. S. Bartolomei[31]. Conditional mutant *Igf1r*$^{fl/+}$ was provided by T. L. Clemens[32]. Interferon-inducible Mx1-Cre or tamoxifen-inducible Scl-Cre mouse strains were used to delete the floxed *H19-DMR* and Igf1r. For Mx1-Cre activation, 250 μg of pIpC was injected intraperitoneally every other day for 14 days at 5 weeks of age. For *Scl-CreER* activation, 2 mg of tamoxifen dissolved in 0.1 ml of corn oil was injected intraperitoneally every day for 5 days.

Single-cell HSC genotyping. Single CD34⁻ Flk2⁻ LSK cells were sorted into 96-well plates (one cell per well) containing 50 μl MethoCult complete media (M3434; Stem Cell Technologies) and incubated (37 °C, 5% CO₂) for 12 days. Individual colonies were collected separately, and DNA was purified using a QIAGENamp DNA Blood Kit (Qiagen). PCR genotyping of *H19* locus used G1, G5 and G7 primers described elsewhere[31].

Flow cytometry. Phenotypic analyses of haematopoietic cells collected from bone marrow (femur and tibia) and peripheral blood were performed as described previously[33,34]. Cell sorting and analysis were performed with a MoFlo (Dako) and/or CyAn ADP (Dako). We analysed data with FlowJo software (Ashland).

5FU treatment. Cohorts of m*H19*$^{ΔDMR/+}$ and m*H19*$^{flDMR/+}$ were injected with 5FU (Sigma-Aldrich) at 150 μg per g (body weight)[34] 4 weeks after pIpC induction. For one cycle, 5FU was injected once intravenously; for three cycles, 5FU was injected three times at 4-week intervals. Bone marrow cells were analysed 10 days after 5FU injections.

Cell cycle analysis. Cell cycle analysis of bone marrow LSKs was performed. Bone marrow cells (5×10^6) were stained for LSKs, fixed overnight at 4 °C in 4% paraformaldehyde and permeabilized with 0.2% Triton X-100. Cells were further stained with a BD Pharmingen™ FITC-conjugated-Mouse Anti-Human Ki67 Set (BD Pharmingen) according to manufacturer's instruction and 0.1 μg μl⁻¹ DAPI. This was followed by flow cytometric analysis with an InFlux Cell Sorter (BD Biosciences).

Transplantation studies. For competitive re-population assays, 2×10^5 bone marrow cells congenic with the host (CD45.1⁺) were included per mouse. One hundred sorted LT-HSCs from m*H19*$^{ΔDMR/+}$ or m*H19*$^{flDMR/+}$ were transplanted intravenously into lethally irradiated (10 Gy) Ptprc (CD45.1) recipient mice. Mice were placed on Baytril water 3 days before irradiation, which continued for 2 weeks after irradiation. Each transplanted group consisted of eight to ten recipients. Donor-derived engraftment was assayed every 4 weeks after transplantation by collection of peripheral blood, red blood cell lysis and staining of CD45.1 (recipient) versus CD45.2 (donor). Multi-lineage reconstitution was determined by CD3, B220 (for T and B lymphoid, respectively) and Gr1, Mac-1 (for myeloid) gating on donor (CD45.2⁺) cells. Limiting dilution experiments were performed by transplanting three doses (200,000, 100,000 and 25,000) of test samples ($n = 2$) from m*H19*$^{ΔDMR/+}$ or m*H19*$^{flDMR/+}$ (CD45.2) with a fixed number of 2×10^5 rescue cells (CD45.2) into groups of ten lethally irradiated (10 Gy) recipient mice (CD45.1). CRU frequency was determined with L-Calc software (Stem Cell Technologies) on the basis of Poisson statistics[35]. The plot was made on the basis of the percentage of recipient mice containing 1% CD45.2⁺ cells in the peripheral blood at 16 weeks after transplantation versus the number of cells injected per mouse. For secondary transplantation, the original, primary transplant recipients were euthanized; bone marrow was collected from the femur and then transplanted mouse-to-mouse at a dosage of 1×10^6 cells per mouse. For reciprocal transplantation, wild-type congenic B6.SJL (CD45.1⁺) bone marrow cells (1×10^6 cells per recipient) were transplanted into lethally irradiated *Mx-1 Cre* induced m*H19*$^{flDMR/+}$ and m*H19*$^{ΔDMR/+}$ (CD45.2⁺) recipients. Complete donor cell engraftment by wild-type CD45.1⁺ cells was confirmed by flow cytometric analysis. For rescue transplants, 2×10^5 (CD45.2) bone marrow cells from the m*H19*$^{flDMR/+}$, *Igf1r*$^{-/-}$ and m*H19*$^{ΔDMR/+}$ *Igf1r*$^{-/-}$ mutants and the controls along with 2×10^5 (CD45.1⁺) Ptprc bone marrow cells were transplanted into CD45.1 recipient mice. Complete donor cell engraftment by wild-type CD45.1⁺ cells was confirmed by flow cytometric analysis.

Lentivirus infection. Mice were treated with 150 μg per g (body weight) of 5FU to activate and enrich for HSPCs[35]. Four days later, bone marrow was collected and cultured overnight in ST media and transduced by Magnetofection™ using ViroMag R/L particles according to the manufacturer's protocol (OZ Biosciences). Transplantation experiments conducted in the knockdown model were done with 300,000 unsorted infected bone marrow cells (CD45.2). The cells were transplanted into each lethally irradiated (10 Gy) Ptprc (CD45.1). Eight weeks after engraftment, bone marrow cells that were double positive for GFP and CD45.2 were sorted for CD34⁻ LSK and CD34⁺ LSK.

Lentivirus construction. The pSicoR-EF1α promoter-IRES-EGFP lentiviral construct was provided by T. Xie.
mir-675: forward, AGCGTGCGGCCCAGGGACTGGTGCGGAAAGGGCCCACAGTGGACTTGGTACACTGTATGCCCTAACCGCTCAGTCCCTGGGTCTGGCA; reverse, GGCATGCCAGACCCAGGGACTGAGCGGTTAGGGCATACAGTGTACCAAGTCCACTGTGGGCCCTTTCCGCACCAGTCCCTGGGCCGCA.
IGF2 shRNA: forward, AGCGCGCCCAAATTTGATTGGCTCTAAATAGTGAAGCCACAGATGTATTTAGAGCCAATCAAATTTGGTCA; reverse, GGCATGACCAAATTTGATTGGCTCTAAATACATCTGTGGCTTCACTATTTAGAGCCAATCAAATTTGGGCG.

Allele-specific Igf2 expression. Male Cast mice were crossed with female flDMR or ΔDMR. Heterozygous progeny at single nucleotide polymorphisms differ between the two strains. In mice that inherited the Cast allele paternally and flDMR maternally, LT-HSCs, ST-HSCs and MPPs were sorted from total bone marrow cells. RNA was extracted and DNase treated using RQ1 RNase-Free DNase according to the manufacturer's instructions (Promega). This RNA was reverse transcribed in the presence of SuperScriptIII Reverse Transcriptase (SSIII) using *Igf2*-specific primer Igf2-20r (5′-gggttgtttagagccaatcaa-3′) according to the manufacturer's instructions (Invitrogen); simultaneously, equal concentrations of RNA were identically treated in the absence of SSIII (for minus (−) RT). Equal volumes of RT and −RT were amplified using 0.5 μM of primers Igf2-18f (5′-atctgtgacctcctcttgagcagg-3′) and Igf2-20r and Go-Taq Green Master Mix (Promega) using the following PCR conditions: 94 °C for 2 min for one cycle; 94 °C for 15 s, 58 °C for 15 s, and 72 °C for 20 s for 43 cycles. No product was detected in −RT samples. Amplified *Igf2* was digested with *Mlu*CI (NEB) and the paternal Cast product (165 base pairs (bp)) and the maternal B6 product (180 bp) were resolved on a 15% polyacrylamide gel similar to methods described earlier[31].

Microarray. RNA was extracted by conventional TRIzol® method from sorted LT-HSCs, ST-HSCs and MPPs (10,000 cells each)[36]. Samples were analysed with Affymetrix MouseGenome430_2 arrays and scanned with a GeneChip Scanner 3000 7G using GeneChip Fluidics Station 450 and GeneChip Operating Software (GCOS 1.4). Heat map data represent the fold change between two populations from at least three independent biological samples. Three samples were run on Affymetrix Mouse 430.2 arrays in triplicate, using the standard Affymetrix protocols. CEL files were read into the R software environment (http://www.cran.r-project.org/) and normalized with RMA[37–39]. Normalized data were fitted with a linear model using the limma package[40] and three contrasts were fitted: CD34p/CD34n, FLK2p/CD34p, FLK2p/CD34n. Probes that were significant for at least one contrast (BH adj $P < 0.05$) went to further analysis.

A list of imprinted genes was taken from the catalogue of imprinting genes at http://igc.otago.ac.nz/1101Summary-table.pdf. Names were matched to MGI and Ensembl 63 genes and then converted to probeset identifications. Of 125 input genes, 86 could be mapped to probesets, and, of these, 23 were significant. Sample expression coefficients per probeset were averaged together by gene. Expression amounts varied widely, from 4 to 14 in log₂ scale, which obscured the regulatory trend across samples during clustering. We constructed a heat map to show only the trending of expression, not the magnitude, by subtracting the mean from each row and dividing by the standard deviation. Thus, the heat map scale shows expression z-scores. Row ordering reflects hierarchical clustering, average linkage, using Pearson dissimilarity for distance. Microarray data have been deposited in ArrayExpress under accession number E-MTAB-1644.

qRT-PCR. Total RNA (2–50 ng) was extracted from sorted LT-HSCs, ST-HSCs and MPPs directly into TRIzol®. This was followed by DNase I treatment (Ambion) and reverse transcription with a high-capacity complementary DNA (cDNA) reverse transcription kit (Applied Biosystems). cDNA was pre-amplified by TaqMan PreAmplification master mix (Applied Biosystems) according to the manufacturer's instructions. TaqMan gene expression assays (Applied Biosystems) were performed on triplicate samples with a 7500 Real-Time cycler (Applied Biosystems). Data were normalized relative to *Gapdh* and *Hprt1*. For mi-R-675-3p assay, extracted RNA were reverse transcribed using TaqMan miRNA reverse transcription kit (Applied Biosystems). TaqMan pre-amplification and TaqMan gene expression assay were performed according to the manufacturer's instructions. All qRT-PCR was performed using TaqMan probes.

Immunostaining. Immunostaining was performed as described previously[33]. For immunostaining of sorted cells, cells were sorted onto lysine-coated slides, fixed with chilled methanol for 10 min, followed by blocking and staining with primary antibody[41]. The following primary antibodies were used: chicken anti Igf1r (Abcam, 1:100), rabbit anti *Igf2* (Abcam, 1:100), rabbit anti FoxO3a (1:100), rabbit anti Foxo1/3/4-Pan and phosphor_Thr24/32 (Assay biotech, 1:50).

RNA-seq. The RNA-sequencing library was prepared from approximately 200 ng of total RNA (m*H19*$^{ΔDMR/+}$ *Igf1r*$^{-/-}$, m*H19*$^{ΔDMR/+}$ *Igf1r*$^{f-/-}$ and m*H19*$^{flDMR/+}$) for each sample using an Illumina TruSeq RNA Sample Prep Kit (catalogue number

FC-122-1001). The fragment size in the generated library ranged from 220 to 500 bp with a pick at 280 bp. A total of 10 fmol library fragments were loaded to cBot to generate clusters, followed by sequencing on an Illumina HiSeq 2000 to produce 10 million to 30 million paired-end 100 bp reads per sample. Reads were trimmed to 70 bp owing to quality and aligned to mm9 with Tophat 1.3.1 (ref. 42)/Bowtie 0.12.7 (ref. 43), using the Ensembl 63 GTF file for gene models. Parameters were −g 1, mate-inner-dist 200, mate-std-dev 70, segment-length 35, segment-mismatches 2; this allowed for four mismatches per read (two per read half) and unique alignments only.

Gene expression was quantified using Cufflinks 1.0.3 (ref. 44). We chose any imprinted genes with an absolute log-fold change of 1.3. A total of 38 imprinted genes were selected this way, 32 having measurements on both samples and six having measurements in only one sample. We heat mapped the genes found in both samples using FPKMs only. For the genes found in both, the range of expression was skewed enough to make visualization by heat map difficult, so we created a row-normalized heat map as with the microarray data. RNA-seq data have been deposited in ArrayExpress under accession number E-MTAB-1628.

31. Thorvaldsen, J. L., Fedoriw, A. M., Nguyen, S. & Bartolomei, M. S. Developmental profile of H19 differentially methylated domain (DMD) deletion alleles reveals multiple roles of the DMD in regulating allelic expression and DNA methylation at the imprinted H19/Igf2 locus. *Mol. Cell. Biol.* **26,** 1245–1258 (2006).
32. Dietrich, P., Dragatsis, I., Xuan, S., Zeitlin, S. & Efstratiadis, A. Conditional mutagenesis in mice with heat shock promoter-driven cre transgenes. *Mamm. Genome* **11,** 196–205 (2000).
33. Zhang, J. *et al.* Identification of the haematopoietic stem cell niche and control of the niche size. *Nature* **425,** 836–841 (2003).
34. Haug, J. S. *et al.* N-cadherin expression level distinguishes reserved versus primed states of hematopoietic stem cells. *Cell Stem Cell* **2,** 367–379 (2008).
35. Miller, C. L. & Eaves, C. J. Expansion in vitro of adult murine hematopoietic stem cells with transplantable lympho-myeloid reconstituting ability. *Proc. Natl Acad. Sci. USA* **94,** 13648–13653 (1997).
36. Akashi, K. *et al.* Transcriptional accessibility for genes of multiple tissues and hematopoietic lineages is hierarchically controlled during early hematopoiesis. *Blood* **101,** 383–389 (2003).
37. Bolstad, B. M., Irizarry, R. A., Astrand, M. & Speed, T. P. A comparison of normalization methods for high density oligonucleotide array data based on variance and bias. *Bioinformatics* **19,** 185–193 (2003).
38. Irizarry, R. A. *et al.* Exploration, normalization, and summaries of high density oligonucleotide array probe level data. *Biostatistics* **4,** 249–264 (2003).
39. Irizarry, R. A. *et al.* Summaries of Affymetrix GeneChip probe level data. *Nucleic Acids Res.* **31,** e15 (2003).
40. Smyth, G. K. Linear models and empirical bayes methods for assessing differential expression in microarray experiments. *Stat. Appl. Genet. Mol. Biol.* **3,** Article3 (2004).
41. Ema, H. *et al.* Adult mouse hematopoietic stem cells: purification and single-cell assays. *Nature Protocols* **1,** 2979–2987 (2006).
42. Trapnell, C., Pachter, L. & Salzberg, S. L. TopHat: discovering splice junctions with RNA-Seq. *Bioinformatics* **25,** 1105–1111 (2009).
43. Langmead, B., Trapnell, C., Pop, M. & Salzberg, S. L. Ultrafast and memory-efficient alignment of short DNA sequences to the human genome. *Genome Biol.* **10,** R25 (2009).
44. Trapnell, C. *et al.* Transcript assembly and quantification by RNA-Seq reveals unannotated transcripts and isoform switching during cell differentiation. *Nature Biotechnol.* **28,** 511–515 (2010).